Atmos. Chem. Phys. Discuss., 14, 32535–32581, 2014
www.atmos-chem-phys-discuss.net/14/32535/2014/
doi:10.5194/acpd-14-32535-2014

Atmospheric Chemistry and Physics Discussions

Ash iron mobilization in volcanic eruption plumes

G. Hoshyaripour[1,2], M. Hort[2], and B. Langmann[2]

[1]Max Planck Institute for Meteorology, Hamburg, Germany
[2]Institute of Geophysics, Center for Earth System Research and Sustainability (CEN), Universität Hamburg, Germany

Received: 3 November 2014 – Accepted: 29 November 2014 – Published: 22 December 2014

Correspondence to: G. Hoshyaripour (gholamali.hoshyaripour@zmaw.de)

Published by Copernicus Publications on behalf of the European Geosciences Union.

Abstract

It has been shown that volcanic ash fertilizes the Fe-limited areas of the surface ocean through releasing soluble iron. As ash iron is mostly insoluble upon the eruption, it is hypothesized that heterogeneous in-plume and in-cloud processing of the ash promote the iron solubilization. Direct evidences concerning such processes are, however, lacking. In this study, a 1-D numerical model is developed to simulate the physicochemical interactions of gas–ash–aerosol in volcanic eruption plumes focusing on the iron mobilization processes at temperatures between 600 and 0 °C. Results show that sulfuric acid and water vapor condense at ∼ 150 and ∼ 50 °C on the ash surface, respectively. This liquid phase then efficiently scavenges the surrounding gases (> 95 % of HCl, 3–20 % of SO_2 and 12–62 % of HF) forming an extremely acidic coating at the ash surface. The low pH conditions of the aqueous film promote acid-mediated dissolution of the Fe-bearing phases present in the ash material. We estimate that 0.1 to 33 % of the total iron available at the ash surface is dissolved in the aqueous phase before the freezing point is reached. The efficiency of dissolution is controlled by the halogen content of the erupted gas as well as the mineralogy of the iron at ash surface: elevated halogen concentrations and presence of Fe^{2+}-carrying phases lead to the highest dissolution efficiency. Findings of this study are in agreement with the data obtained through leaching experiments.

1 Introduction

In 2010, sockeye salmon unexpectedly reached record numbers in British Columbia's Fraser River after low numbers during recent decades (Larkin, 2010). It has been hypothesized that the soluble iron contained in the volcanic ash from the eruption of Kasatochi volcano, Aleutian Islands, in 2008, could have indirectly provided a feast for the salmon (Parsons and Whitney, 2012) through an enhanced marine primary productivity and phytoplankton bloom upon ash deposition into Fe-limited ocean surface

ACPD
14, 32535–32581, 2014

waters (Olgun et al., 2013a). This phytoplankton bloom was indeed the first direct evidence of a fertilization effect of volcanic ash iron on the surface ocean (Langmann et al., 2010; Hamme et al., 2010). It is also reported recently that the dissolved iron released from volcanic ash triggers small scale but significant perturbations in the marine biogeochemistry (Olgun et al., 2013b; Achterberg et al., 2013). However, knowing the fact that the ash iron near the volcanic vent is mostly insoluble (as a component of the glass and as primary Fe-bearing silicate and Fe-oxide minerals, (Heiken and Wohletz, 1992)), it is not yet fully understood which processes solubilize the iron during ash transport from the volcano to the ocean.

Volcanic ash is the tephra with a diameter < 2 mm (Rose and Durant, 2009) typically composed of silicate glass and crystalline materials generated by fragmentation of the rising magma as well as erosion of the conduit wall rock (Heiken and Wohletz, 1992). While physical properties of the ash (size distribution, specific surface area etc.) are usually dictated by the fragmentation and eruption mechanism, its bulk mineralogy and composition are controlled by cooling and crystallization of the source magma (Dingwell et al., 2012).

During its journey from the fragmentation to high altitudes in the atmosphere and finally to the surface ocean, ash undergoes numerous physicochemical processes through various environmental conditions that can be categorized as in-conduit, in-plume and in-cloud (Table 1). As a result, the surface of the ash does not necessarily mirror the mineralogy and composition of the source magma since it constantly interacts with volcanic gases, aerosols and ambient air (Horwell et al., 2003; Delmelle et al., 2007). For instance, Bagnato et al. (2013) observed a significant difference between surface chemical compositions of proximal and distal ash deposits of Eyjafjallajökull eruption in 2010, Iceland. These alterations in the ash surface composition are attributed to the in-plume and in-cloud processing of volcanic ash (Bagnato et al., 2013). Reviews of such processes are provided, for e.g., by Textor et al. (2005). Here we briefly summarize those processes that are relevant for ash iron mobilization during

ACPD
14, 32535–32581, 2014

plinian and sub-plinain eruptions (for a detailed review please see Ayris and Delmelle, 2012).

In-conduit processes refer to high-temperature post-fragmentation subterranean gas–ash interaction. Large explosive eruptions with deep magma fragmentation are likely to be affected by significant in-conduit gas–tephra interaction at temperatures above 600 °C (Ayris et al., 2013). Such interactions can account for SO_2 scavenging by glass-rich tephra that proceeds by a Ca^{2+} diffusion-driven mechanism (Ayris et al., 2013). It is also suggested that high-temperature HCl adsorption prior to the mixing of the erupted material with the ambient air could produce minor quantities of Fe-bearing salts on the ash surface (Ayris et al., 2014). Although these findings provide valuable experimental evidences, such processes cannot be considered as the dominant mode of iron mobilization since the suggested quantities are far from explaining the soluble iron required for the observed ocean fertilizations (Langmann et al., 2010). Besides, eruption conditions required for such high-temperature processes to become dominant (e.g., conduit ascent time of more than some hundreds of seconds, (Ayris et al., 2014)) seem to be rare.

In-plume processes encompass a wide range of temperature (from magmatic temperatures down to ambient temperature) and distance (from the vent up to the neutral buoyancy level (NBL)) during which the volcanic ejecta is mixed with the ambient air. As shown in Table 1, we can identify three temperature-dependent sub-zones within the in-plume region: high-, mid- and low-temperature (here after referred to as high-, mid- and low-T). Hoshyaripour et al. (2014) investigated the high-T in-plume processes ($T > 600$ °C) through modeling the direct gas–ash interactions governed by mixing of the magmatic gas and ash with the ambient air. They reported that such processes do not solubilize the iron directly but significantly control its mineralogy and oxidation state at the ash surface within a 100 nm thick rim. They emphasized that further in-plume and in-cloud processes can play the dominant role in ash iron mobilization.

Mid- and low-T reactions ($T < 600$ °C) within the eruption plume could alter the ash surface composition, and thus potentially influence further (photo)chemical reactions

ACPD
14, 32535–32581, 2014

during transport of ash in the atmosphere (Ayris and Delmelle, 2012). It is suggested that sulfuric acid condenses first which is then followed by water condensations in the cloud zone (Óskarsson, 1980). This procedure develops an acidic coating on the ash surface that is expected to dissolve the ash iron efficiently (Delmelle et al., 2007). In-cloud processing of volcanic ash, which is mainly governed by heterogeneous reactions involving liquid water and ice, could also mobilize the insoluble iron contained in the ash surface through, for e.g., dissolution/precipitation and freezing/melting cycles (Duggen et al., 2010). Ayris and Delmelle (2012) speculated that these processes could eventually lead to formation of soluble Fe-sulfate/chloride/fluoride salts on the ash surface. However, direct theoretical and experimental evidences supporting these hypotheses are required.

Previous modeling investigations on physical chemistry of volcanic eruption plumes have mainly focused on gas chemistry (e.g., Bobrowski et al., 2007), micro-physical processes like condensation, scavenging and freezing (Tabazadeh and Turco, 1993; Textor et al., 2003) and also particle aggregation (Textor et al., 2006b, a) leaving the chemical interactions of the aqueous phase and the ash surface nearly unexplored. As a result, despite of advancements made by individual studies, a detailed insight into the in-plume and in-cloud processes that promote the iron mobilization in volcanic ash remains lacking. This study therefore aims to investigate the role of these processes in ash iron mobilization through numerical modeling of gas–ash–aerosol interactions. The main objectives are (1) to find out how much iron (ferrous and ferric) is mobilized from the ash surface (dissolved in the aqueous phase) during its vertical transportation within the eruption plume and (2) to identify the favorable conditions/processes for iron mobilization in volcanic ash. In the following sections, first the modeling concepts and methods are presented. Then the results of the simulations and their sensitivity to different parameters are discussed. Finally the results are compared with experimental measurements and conclusions are given.

ACPD
14, 32535–32581, 2014

2 Methodology

2.1 Modeling framework

Figure 1 shows the main in-conduit, in-plume and in-cloud interactions of gas–ash–aerosols. In-conduit and high-T in-plume zones (zones 0 and 1 in Fig. 1) have been investigated previously (Hoshyaripour et al., 2014; Ayris et al., 2013, 2014). In this study we explore mid- and low-T in-plume and warm in-cloud zones (zones 2, 3 and 4 in Fig. 1, respectively) through a simplified 1-D modeling approach. In other words, the lower boundary is the material leaving the high-T zone and entering zone 2 ($T = 600\,^{\circ}\mathrm{C}$) and the upper boundary is the output of zone 4 ($T \sim 0\,^{\circ}\mathrm{C}$). Sulfuric acid condenses first (at the boundary between zones 2 and 3) followed almost immediately by water condensation (at the boundary between zones 3 and 4) and thus, dissociates to H^+ and HSO_4^- where we can assume that the processes are similar to conventional in-cloud processes considered in atmospheric sciences (Seinfeld and Pandis, 2006). In this study we assume that ash particles are active as condensation nuclei for sulfuric acid and water condensation (Textor et al., 2006b).

Since freezing has a significant impact on the physicochemical interactions (Textor et al., 2003), we consider two subsections for the in-cloud zone: warm (without ice/before freezing) and cold (with ice/after freezing). In the warm in-cloud zone, the aqueous phase scavenges volatiles (e.g., HF, HCl and SO_2) from the surrounding atmosphere and also dissolves the constituents of the ash surface. These processes release cations (e.g., Na^+, Fe^{2+}, Al^{3+}) and anions (e.g., Cl^-, SO_4^-, F^-) into the liquid phase, which can react with each other generating soluble salts (Stum and Morgan, 1996). When the temperature of the system reaches to freezing point (cold in-cloud or zone 5 in Fig. 1), ice forms at the ash surface and interacts with the surrounding atmosphere (Textor et al., 2003) and also with the ash surface. This zone is however beyond the scope of this study.

Approximate temperature ranges associated with different zones are shown in Fig. 1 and discussed in Sect. 3. It is noteworthy that these boundaries can slightly change

ACPD
14, 32535–32581, 2014

according to the atmospheric conditions and eruption dynamics and also may have some overlap with each other. For instance, the presence of ions in the liquid phase can cause a depression in saturation vapor pressure and shift the freezing point to lower temperatures leading to super-cooled water formation (Tabazadeh and Turco, 1993). Nevertheless, these are reasonable boundaries to better distinguish the role of different environmental conditions on gas–ash–aerosol interactions.

2.2 Dynamics of the eruption plume

Considering the great diversity in style of volcanic eruptions, there are different mechanisms for mixing of volcanic gas, ash, and atmospheric gases. Mixing itself is controlled by temperature and eruption dynamics (turbulence and air entrainment). Here we focus on the mixing processes in sub-plinian and plinian eruption plumes in which air entrainment reduces the density and also the temperature of the plume. As a first order approximation, the travel time from the vent to the NBL is 150–250 s during which the plume temperature is lowered by $\sim 1000\,^{\circ}\mathrm{C}$ (Hort and Gardner, 2000). Thus, the mixture cooling rate is in the range of $4–7\,^{\circ}\mathrm{C\,s^{-1}}$ in the convective region of the plume. As a reference atmosphere we use the standard atmosphere having a sea level temperature of $0\,^{\circ}\mathrm{C}$, a thermal lapse rate in the troposphere of $6.5\,\mathrm{K\,km^{-1}}$, a troposphere thickness of 11 km, a 9 km-thick tropopause, and no humidity according to US Committee on Extension to the Standard Atmosphere (1976). Since processes involving ice ($T < 0\,^{\circ}\mathrm{C}$) and stratospheric processes are beyond the scope of this study, we set $0\,^{\circ}\mathrm{C}$ plume temperature and/or 11 km as the upper boundary of our model. Assuming a vent altitude of 1 km together with the average rise time of 200 s, we obtain an average cooling rate of $5\,^{\circ}\mathrm{C\,s^{-1}}$ and an average ascent velocity of $50\,\mathrm{m\,s^{-1}}$ for our reference scenario, both values being well in the range suggested in the literature (cooling rate of $4–7\,^{\circ}\mathrm{C\,s^{-1}}$ (Hort and Gardner, 2000) and plume ascent velocity of $40–80\,\mathrm{m\,s^{-1}}$, Mastin, 2007). The results discussed below are not sensitive to these particular parameter values over a wide range of variation. At each step, temperature and elevation of the plume are calculated as prognostic variables based on these presumed rates

ACPD
14, 32535–32581, 2014

while pressure as well as the kinetic and thermodynamic reaction rates are derived as diagnostic variables.

2.3 Mass balance equations

Concentrations of gas- and particulate-phase species in the plume are determined by solving a system of coupled mass balance equations. In its most general form, this equation is (Meskhidze et al., 2005):

$$\frac{\mathrm{d}}{\mathrm{d}t}[C_i] = P_i - D_i - \alpha_{\mathrm{dep}}[C_i] - \alpha_{\mathrm{dill}}[C_i] \quad i = 1, \ldots, n \tag{1}$$

where C_i is the concentration of species i within the plume in $\mathrm{mol\,m^{-3}}$, P_i and D_i are production and destruction rates for species i in $\mathrm{mol\,m^{-3}\,s^{-1}}$, α_{dill} is a rate constant for dilution of the plume due to mixing with ambient air, α_{dep} is the rate constant for loss of species contained within ash and aerosols due to fallout and deposition (wet and dry) and n is the number of species considered (see Table 2). In this study we focus on calculation of the terms P_i and D_i via kinetic and thermodynamic reactions between gases, aqueous phase and the ash surface. The term α_{dill} is calculated based on the expansion of the plume due to air entrainment, temperature and pressure changes following the equation of state. As we focus on in-plume and warm in-cloud processes with time scale of few seconds to few minutes (see Table 1), for simplicity we can safely neglect the term α_{dep} for the fine ash. At each step, a system of n ordinary differential equations (ODE) is solved using the ode15s solver in MATLAB (Shampine and Reichelt, 1997). All considered gas-phase reactions and their rate parameters are listed in the appendix (Table A1).

Beside kinetic reactions in the gas phase, processes like condensation of sulfuric acid and water as well as the dissolution of the ash in the aqueous phase are among the most important P_i and D_i terms in this study which are explained below.

ACPD
14, 32535–32581, 2014

2.4 Condensation

At mid temperatures (150 °C < T < 600 °C) in the eruption plume, heterogeneous reactions involving the gas phase and the ash material take place. Although the direct emission of H_2SO_4 is small, some of the SO_2 oxides to SO_3, which upon cooling readily reacts with water vapor to form vapor-phase sulfuric acid (H_2SO_4) (Hoshyaripour et al., 2012). As cooling continues, the temperature eventually drops below the dew point of the gas mixture, allowing condensation of H_2SO_4 onto the ash surfaces. Sulfuric acid has the highest dew point of all magmatic gas constituents and therefore, always condenses first (Verhoff and Banchero, 1974). Details of calculating the sulfuric acid condensation rate are given in Appendix A1.

As soon as the saturation vapor pressure of water vapor is reached, liquid water condensation on the ash surface takes place. Since water vapor concentration is at least 3 orders of magnitude higher than that of H_2SO_4 in magmatic gas (Symonds et al., 1994), it readily dissociates the condensed sulfuric acid into H^+ and HSO_4^-. This process can eventually lead to high concentrations of dissolved H_2SO_4 in the condensate associated with the ash, and thus, to strongly acidic pH values on the ash surface (Ayris and Delmelle, 2012). Rate parameters of water condensation are summarized in Appendix A2.

2.5 Thermodynamic equilibrium

Once the concentrations of the major species listed in Table 2 have been determined at a given time step using the equations described above, these species must be speciated into their various possible chemical forms. This is accomplished in the model by invoking thermodynamic equilibrium between the gas and liquid phase. We use the mass flux iteration method (MFI) to solve for thermodynamic equilibrium (Jacobson, 2005). MFI solves each equilibrium equation iteratively and iterates over all equations while conserving mass and charge (for more details see Jacobson, 2005). The thermodynamic equilibrium reactions considered in this study (dissolution and dissocia-

ACPD
14, 32535–32581, 2014

tion) and the parameters for calculating their equilibrium coefficient are presented in Appendix A3

2.6 Ash dissolution

The liquid film or droplets at the ash surface not only scavenge the volatiles from the gas but also dissolve the ash surface constituents. This dissolution process eventually results in formation of Fe^{2+} and Fe^{3+} in the aqueous phase (together with other cations and anions), which is central to further in-cloud processes. Ash dissolution rate calculations used in this study are presented in Appendix A4.

2.7 Size distribution of the ash

Particle sizes < 1 mm are considered in this study, which corresponds to the definition of fine ash (Rose and Durant, 2009). Fine ash is thought to represent a substantial contribution (50–97 wt%) to tephra deposits from plinian and sub-plinian volcanic eruptions (Rose and Durant, 2009). Particles in this size range not only have a higher surface to mass ratio (compared to the coarser particles) for interaction with the gases and aqueous phases (Delmelle et al., 2005) but also can be lifted to high altitudes and remain suspended in the atmosphere for several days before sedimentation (Sparks et al., 1997). Among others, Rose and Durant (2009) investigated the ash content of volcanic eruption plumes and suggested a typical polymodal size distribution for fine ash subdivided into 27 bins (Fig. 2a). For this binned representation of fine volcanic ash, the total number of bins between 0.01 to 1000 µm (see Fig. 2a) is denoted by nclass. Each bin i is considered to be monodisperse with a radius R_p^i which is given by the following equation (Pirjola et al., 1999):

$$\log_{10}(R_p^i) = \log_{10}(r_{\min}) + \frac{\log_{10}(r_{\max}) - \log_{10}(r_{\min})}{\text{nclass}}(i-1) \quad (2)$$

ACPD
14, 32535–32581, 2014

Here we use nclass = 27 (Fig. 2a). Using R_p^i and an ash density of 2300 kg m^{-3} (Rose and Durant, 2009), we calculate the mass of a single particle in each bin. Assuming that near the vent approximately 3 wt% of the plume is gas and about 97 wt% is ash (Sparks et al., 1997), for each mol of volcanic gas (with an average weight of 25 g), the erupted material contains approximately 830 g ash, which at T = 1000 °C and P = 1 bar corresponds to in-plume ash concentration of 0.005 g cm^{-3} near the vent. Finally, using wt% of each size bin (Fig. 1a), the mass of a single particle and the ash concentration calculated above, we compute the number of particles in each bin per cm^3, which is shown in Fig. 2b. According to this plot, we estimate the total number concentration near the vent to be approximately 10^{12} particles cm^{-3} having a total surface area of ash 45 cm^2 cm^{-3}. According to previous studies, the specific surface area of fine volcanic ash is in the range 0.2–2.1 m^2 g^{-1} (Delmelle et al., 2005; Mills and Rose, 2010). We find 0.9 m^2 g^{-1} as the specific surface area of the fine ash in this study, which is well in the range mentioned above.

2.8 Initial gas and ash composition

It is known that convergent plate volcanism is more likely to generate plinian and sub-plinian eruptions (Schmincke, 2004) in which huge amounts of fine ash are released and could be transported thousands of kilometers to reach the oceans (Duggen et al., 2010). Therefore, we consider the magmatic gas composition of convergent plate (CP) volcanoes as the reference scenario for this study (CP composition in Table 3). This composition reflects the magmatic gas and air mixture leaving the hot core of the plume (T > 600 °C or zone 1 in Fig. 1), and is taken as the input into our modeling study which focuses on 0 °C < T < 600 °C.

Iron at the ash surface leaving the high-temperature zone mainly occurs as component of glass and as Fe-carrying phases mentioned in Table 2 (Bayhurst et al., 1991; Nakagawa and Ohba, 2003). For simplicity, ash in this reference scenario consists of magnetite (Fe_3O_4) as the Fe-carrying mineral. Magnetite contains iron in both oxida-

ACPD
14, 32535–32581, 2014

tion states (ferric and ferrous) and is considered as an iron oxide with intermediate oxidation state. Its presence in volcanic ash is also reported in analytical (Nakagawa and Ohba, 2003) studies. Other minerals as well as silicate glass are considered in a detailed sensitivity study in Sect. 4.2.

3 Results

3.1 In-plume zones: water and sulfuric acid condensation

Figure 3 shows the vertical profile of water and sulfuric acid in both vapor and liquid phases. Left and right *y* axis show the plume elevation and the temperature, respectively. H_2SO_4 condenses first at ∼ 120 °C (boundary between mid- and low-T in-plume zones). The conceptual model of Óskarsson (1980) suggests the temperature of 338 °C as the condensation point of sulfuric acid corresponding to the dew point of pure H_2SO_4 at 1 bar (Verhoff and Banchero, 1974). However, this value is too high for volcanic plumes considering the low mixing ratio of H_2SO_4 in the gaseous phase (< 1 mol%) as well as the low pressure at high elevations in the atmosphere.

The concentration of sulfuric acid droplets increases and reaches a plateau near 40 °C (boundary between in-plume and in-cloud zones). At this point water vapor starts condensing which is followed by rapid depletion of H_2SO_4 due to its dissociation in contact with liquid water (see Fig. 3a). At $T < 50$ °C gaseous sulfuric acid continues to condense (H_2SO_4(g) in Fig. 3a) and dissociate rapidly into H^+ and HSO_4^-, thus no liquid H_2SO_4 forms anymore (H_2SO_4(aq) in Fig. 3b). More than 80 % of the sulfuric acid (all fractions given in this paper are mass fractions) condenses in the low-T in-plume and warm in-cloud zones.

We note that the eruption dynamics and gas composition can slightly vary the boundaries of mid- and low-T in-plume zones. Based on several simulations conducted in the course of this research we suggest average values of 150 and 50 °C for H_2SO_4 and H_2O condensation point in volcanic plumes, respectively. It is also noteworthy that the

ACPD
14, 32535–32581, 2014

altitudes at which the plume reaches these temperature-dependent boundaries are significantly variable in different eruptions.

3.2 Warm in-cloud zone

3.2.1 Scavenging of gases

It has been observed that volcanic particles scavenge gas species in volcanic eruption plumes (Rose, 1977; Óskarsson, 1980). Water condensation generates a liquid coating on the ash surface (in the warm in-cloud zone) that scavenges the surrounding gases (Textor et al., 2003). Since the solubility of HCl is about four orders of magnitude higher than that of SO_2, it is likely to be completely scavenged by water drops (Tabazadeh and Turco, 1993) thereby increasing the acidity of the aqueous phase and consequently decreasing SO_2 scavenging which is observed in our simulations (Fig. 4, right panel). While more than 98 % of the HCl is removed from the gas phase, only less than 5 % of the SO_2 is scavenged by the liquid water in the reference scenario. Therefore, in consistency with previous studies (Tabazadeh and Turco, 1993; Textor et al., 2003), high fractions of SO_2 can reach the stratosphere, while a much lower fraction of HCl remains in the gas phase.

In general, the solubility of acid gases decreases with increasing acidity of the aqueous phase (Atkins, 1986). Since HCl dissolves more efficiently, it increases the acidity of the aqueous phase and hinders SO_2 scavenging. Neglecting HCl scavenging (Fig. 4, left panel), which can also represents eruptions with very low halogen content, increases the SO_2 removal from the gas phase to 15 %.

As noted before, dissolution of the major gas species in the aqueous phase is usually followed by their rapid dissociation (see E8 to E14 in Table A2). Figure 5 shows the major products of the dissociation processes. Formation of all these anions is concurrent with H^+ release in the aqueous phase, which increases the acidity of the solution. Since Cl^- has the highest concentration (2 to 9 order of magnitudes greater than that of other anions), HCl dissolution and dissociation mainly control the pH. The final pH of

ACPD
14, 32535–32581, 2014

the liquid phase in the reference scenario is 0.32 (extremely acidic), which significantly affects the ash dissolution efficiency discussed below. HSO_4^-, HSO_3^- and F^-, which form due to dissociation of H_2SO_4, SO_2 and HF, respectively, are the more abundant species following Cl^-.

3.2.2 Ash dissolution

The condensation, dissolution and dissociation processes in the plume acidify the liquid coating on the ash surface which dissolves the minerals and other solids (e.g., silicate glass). Figure 6 shows the dissolved iron (ferric and ferrous) from magnetite in the reference scenario. The acidic liquid phase ($pH < 0.5$) dissolves magnetite in the ash with an average dissolution rate of $6.44 \times 10^{-12}\,mol\,cm^{-2}\,s^{-1}$, which is in the range reported in experimental studies (Delmelle et al., 2007). This process consumes H^+ and produces cations (Fe^{2+} and/or Fe^{3+}), which can also react with the anions in the aqueous phase and generate soluble iron salts. These salts can precipitate at the ash surface after water has evaporated. This is supported by the fact that surface of the ash particles are coated by a thin layer of salts in the form of iron sulfates and iron halides in the eruption plume (Naughton et al., 1974; Delmelle et al., 2007).

Only 0.15 % of the total surficial magnetite is dissolved which releases Fe^{2+} and Fe^{3+} in the aqueous phase. Although the relative quantity of the dissolved iron seems very small, one has to take into account that huge amounts of ash are usually erupted during major eruptions. This is further discussed in Sect. 5.1.

4 Sensitivity analysis

4.1 Gas composition (tectonic setting)

It is suggested that there is a correlation between tectonic setting of volcanoes and the iron release from their ash upon contact with seawater (Olgun et al., 2011). To evaluate

ACPD
14, 32535–32581, 2014

this hypothesis, we use gas compositions of three types of volcanic settings: convergent plate (CP), divergent plate (DP) and hot spots (HS) (Table 3) which tend to emit chlorine-rich, carbon-rich and sulfur-rich gases, respectively (Symonds et al., 1994). The CP composition is the same as the reference scenario discussed above. The ash is assumed to be composed of magnetite in all these scenarios. Table 4 shows the key parameters relevant to iron mobilization calculated during the sensitivity analysis. It can be seen that the dissolution rate, pH and total dissolved iron are in the same orders of magnitude for different gas compositions and vary by 10–20 %.

In all tectonic settings, HCl is almost readily scavenged by the aqueous phase which consequently controls the HF and SO_2 scavenging, pH of the liquid and finally the dissolution rate. In the CP setting the lowest pH and the highest dissolved iron and dissolution rate is attained. Figure 7 shows the changes in pH vs. HCl concentration in the gas phase and also the dissolution rate. It can be seen that the HCl scavenging controls the pH of the system and consequently the dissolution rate. Therefore, Cl-rich magmatic gases (typically the CP volcanism) could be favorable for mobilizing the ash iron. This will be further discussed in Sect. 5.2.

4.2 Ash composition

One important aspect of this study is that ash contains different minerals (and not only magnetite as assumed above) as well as considerable amounts of silicate glass. In this section, the effect of ash mineralogy and composition on iron mobilization efficiency is discussed. Fe-carrying phases, being precipitated under more reduced and oxidized conditions in the source magma include olivin (here fayalite will be the iron carrying phase), and hematite, respectively (Nakagawa and Ohba, 2003). Moreover, silicate glass, which is a major component of volcanic ash, contains iron in an amount equivalent to the original magma prior to eruption. Since the iron content of fayalite, hematite and magnetite is much higher than that of the glass, we can safely neglect the iron release from the glass due to its dissolution. Thus, glass acts only as a sink for H^+ and can represent the effect on other ash constituents on H^+ consumption. Table 4 shows

ACPD
14, 32535–32581, 2014

the results of the control run in which gas composition remains constant (CP in Table 3) and magnetite is replaced by four different ash compositions:

A. 100 % glass,

B. 70 % glass + 30 % hematite,

C. 70 % glass + 30 % fayalite,

D. 70 % glass + 10 % hematite + 10 % fayalite + 10 % magnetite.

In the scenarios that include pure glass and glass + hematite (compositions A and B), the pH and the amount of scavenged SO_2 and HF are not significantly different from that of the reference scenario (CP in Table 4). The dissolution rates of the glass and hematite are 7 and 1 order of magnitude smaller than that of magnetite (the reference scenario), respectively. For the compositions including fayalite at the ash surface (compositions C and D), significant changes in pH, SO_2 and HF scavenging are observed. Since the fayalite dissolution rate is 2 orders of magnitudes greater than that of magnetite (reference scenario), 33 and 13.85 % of the total iron is dissolved in the aqueous phase in the warm in-cloud zone for compositions C and D, respectively. Such an elevated dissolution rate consumes H^+ more rapidly (see Table 4), reduces the acidity and consequently enhances the SO_2 and HF scavenging. This increases the SO_2 and HF scavenging from 2.8 and 12.5 to 19.6 to 61.55 %, respectively. The subsequent dissociation of the SO_2 and HF can increase the acidity again and intensify the ash dissolution. This cycle can dominantly promote the ash iron mobilization.

These results may suggest that volcanic settings that buffer iron mainly as Fe^{2+} in the ash surface (reduced magmatic conditions at DP and HS volcanism, Hoshyaripour et al., 2014) could eventually lead to very high iron mobilization rates. This is further discussed in Sect. 5.2.

ACPD
14, 32535–32581, 2014

5 Discussion

5.1 Comparison with experimental data

Based on the results presented above, acid-mediated dissolution of the ash seems to be the major process that mobilizes the ash iron. Dissolution and dissociation of halides (HCl and HF) in the aqueous phase mainly control its pH and therefore, ash dissolution efficiency (see Fig. 7). The crucial role of chlorine and fluorine in enhancing ash dissolution reactions has been emphasized previously (Delmelle et al., 2007; Wolff-Boenisch et al., 2004; Moune et al., 2007). It has been suggested that the ash dissolution is most efficient within the eruption plume possibly occurring during the first minutes of the transport dictating the surface composition of ash (Moune et al., 2006; Delmelle et al., 2007). The fingerprint of these in-plume processes (namely the preferential enrichment of Cl and F on tephra surfaces) is dominant in proximal samples that deposit before being significantly affected by cloud processes (Delmelle et al., 2007). Therefore, we use proximal samples data obtained in experimental studies to evaluate the correlation between pH, halide and iron release from the ash. Jones and Gislason (2008) measured the concentrations and fluxes of elements into de-ionized water through leaching experiments on 8 unhydrated volcanic ash samples. Five ash samples (Galeras, Montserrat, Hekla, Sakura-Jima and Lascar) are selected for evaluation in this study since they are collected < 15 km away from the vents and thus, could be considered as proximal samples (for more details see Jones and Gislason, 2008).

Figure 8 shows concentration of iron and halides (Cl+F) released from ash samples as a function of pH. This figure unambiguously shows the higher the chlorine and fluorine concentrations, the lower the pH and the higher the iron release. The absolute pH values in this figure are higher than those calculated in this study (Table 4) because ash samples are influenced by freezing/melting, precipitation/evaporation cycles as well as aqueous chemistry during further in-cloud processing, which are not considered in our model simulations. All these processes may change the absolute pH values and also

ACPD
14, 32535–32581, 2014

iron and halide speciation. However, their relative quantities still buffer the correlation of pH, iron dissolution efficiency and the chlorine and fluorine concentrations.

The ash sample from Hekla has two orders of magnitude higher iron release than those of the other samples. The reason of this exceptional iron release from Hekla ash stems mainly from its unusual composition (erupted gas and ash composition), with a combined hotspot and divergent plate margin magma source, coupled with high fluorine in the eruptive products (Óskarsson, 1980; Moune et al., 2006). Petrological estimates suggest reduced conditions for the basaltic Hekla magma prior to eruption (Moune et al., 2007). As a result, the observed mineral phases in the Hekla ash include olivine, clinopyroxene and spinel (Höskuldsson et al., 2007), which is close to the C and D ash compositions in Table 4. As discussed above, having Fe^{2+}-carrying species and high halide content concurrently in the eruption plume can mobilize 13.85–33 % of the total iron at the ash surface. Since there is no evidence for such exceptional conditions for the other eruptions considered in Fig. 8, we use the range of 0.03–0.15 % (according to the ash composition B and the CP gas composition in Table 4, respectively) as the wt% of mobilized surficial iron in these samples. To estimate the iron release from ash R_{Fe} (mol g^{-1} ash) based on proposed theoretical values in this study, the following equation is used:

$$R_{Fe} = C_{Fe} I_s D_i / M_{Fe} \quad (3)$$

where C_{Fe} is the iron wt% in the bulk composition, I_s is the ash surface layer weight ratio (1–5 % of the total ash mass), D_i is the wt% of the dissolved iron according to Table 4 and M_{Fe} is the molar weight of iron (55.84 g mol^{-1}). The R_{Fe} values calculated in this study and also measured by Jones and Gislason (2008) are shown in Table 5. The measured iron release from four ash samples is satisfactorily in the calculated range based on Eq. (3). Only the Galeras ash is slightly outside the range. Therefore, according to Fig. 8 and Table 5 there is a good overall agreement between the results of the theoretical approach of this study and experimental measurements of ash iron

ACPD
14, 32535–32581, 2014

release. This confirms the strong connection between iron release from ash with the halide concentrations and pH.

The relative quantity of the mobilized iron discussed above may seem minor (especially the 0.03–0.15 % in the reference scenario). But this needs to be considered in the context of the massive ash content of the volcanic ejecta. For instance, the eruption of Kasatochi volcano in 2008 produced approximately 6×10^{11} kg of ash (Langmann et al., 2010) containing 5–10 wt% iron in the bulk composition (Wang et al., 2010). Assuming the mass of the ash surface rim as approximately 1–5 % of the total mass, the surface rim of the ash from Kasatochi eruption carries approximately 0.6–3 × 10^8 kg iron. Mobilization of 0.03–0.15 % of the iron at the ash surface (as in the reference scenario) according to Eq. (3) means 5–134 nmol Fe g^{-1} ash which is close to the measured iron released from Kasatochi ash (61–81 nmol Fe g^{-1}) reported by Olgun et al. (2013b). Although the fate and speciation of the dissolved iron depend on further in-cloud processes, the calculations above indicate that even a very small percentage of mobilized iron in the ash means a huge mass with potentially significant impacts on the receiving environment.

5.2 Favorable conditions for iron mobilization

Duggen et al. (2010) and later, Olgun et al. (2011) reported a correlation between tectonic setting and ash iron fertilization suggesting the subduction zone (convergent plat) volcanism as the favorable setting for soluble iron production. However, in their comparisons, they neglected the exceptionally high iron release from the ash of the Hekla eruption in 2000. The distribution of their sample seems also statistically biased toward CP volcanism as they analyzed 40 samples form CP volcanoes and only 4 samples form HS setting. Emissions from CP volcanism are known to be Cl-rich (Symonds et al., 1994). Thus, according to the results of this study, development of highly acidic coatings on the ash surface is very likely in CP eruptions resulting in elevated ash dissolution rates. The efficiency of acid-mediated dissolution however, depends not only on acidity and temperature but also on the mineral composition (Blesa et al., 1994). Fe^{2+}-carrying

ACPD
14, 32535–32581, 2014

phases (reduced iron minerals) show higher dissolution rates under acidic conditions (see Sect. 4.2 and also, Palandri and Kharaka, 2004). Non-arc settings (DP and HS) typically record reduced conditions in comparison to the CP setting (Lindsley, 1991). Thus, DP and HS settings could be favorable for iron fertilization too with respect to iron oxidation state. Hekla eruption in 2000, Iceland, had both reduced magmatic conditions (as usual for DP and HS) and high halides content (as usual for CP) (Moune et al., 2009) which leads to an exceptional iron release behavior. Therefore, our results suggest that attributing the fertilization potential of the ash to the tectonic setting of volcano is an inconsistent hypothesis. Instead, elevated halide content in the gas (HCl and HF) and reduced conditions in the magma seem to be the favorable conditions for ash iron mobilization.

6 Conclusion and implications

The 1-D numerical model introduced in this study simulates the heterogeneous interactions of the gases, liquid phase and the ash surface within the volcanic eruption plume in the temperature range of 600 to 0 °C. It provides the first theoretical constraints on the impacts of such processes on ash iron mobilization. Although determining the fate of the dissolved species in the aqueous phase requires further investigations, our first attempt reveals that the ash dissolution can even modulate the gas scavenging efficiency through changing the pH of the liquid coatings. Therefore, ash needs to be considered as a reactive component in modeling the physical chemistry of volcanic eruption plumes and clouds.

According to our results, in eruption plumes with high halogen content (CP volcanism), dissolution and dissociation of HCl (and partly HF) mainly controls the pH of the aqueous phase at the ash surface in the warm in-cloud zone. For these volcanoes SO_2 scavenging by liquid particles could be negligible and seems to be more efficient in contact with ice particles as suggested by Textor et al. (2003). On the other hand, during sulfur rich eruptions (DP and HS volcanism) SO_2 scavenging by the aqueous

ACPD
14, 32535–32581, 2014

phase is more likely and could be the main process controlling the pH and thus, ash dissolution.

Under acidic pH conditions, the dissolution of iron oxides could be greatly enhanced in the ice phase compared to that in water (Jeong et al., 2012). As dissolution consumes H^+, it reduces the acidity and can accelerate the SO_2 scavenging by ice (Textor et al., 2003). Therefore, sulfur scavenging by volcanic ash and aerosols seems to be less efficient during mid- and low-T in-plume as well as the warm in-cloud processes. Instead, high-T (both in-conduit, Ayris et al., 2013, and in-plume, Hoshyaripour et al., 2014) and cold in-cloud zones (Textor et al., 2003) appear to be more relevant to the sulfur scavenging. These effects should be considered in interpreting the results of leaching experiments on ash deposits to distinguish the fingerprint of the in-plume and in-cloud processes on the ash surface composition.

The local, regional and global impacts of volcanism upon the Earth system (atmosphere, hydrosphere, pedosphere, cryosphere and biosphere) are initially induced by the physicochemical properties of the ash and gas. Several lines of evidence indicate that the in-plume and in-cloud processes can significantly alter these properties and thus, their impacts on Earth system. Therefore, the in-plume and in-cloud processing of the volcanic ejecta need to be considered in future investigations on, for e.g., injection of volcanic gases into the stratosphere and its climatic impacts.

In addition to the ash and gas composition, which are largely governed by the composition of the source magma, other factors can considerably vary the efficiency of iron mobilization at the ash surface. Particle size distribution basically controls the surface area to mass ratio, which is a key parameter for condensation, scavenging and dissolution processes. Smaller particles with lower surface area to mass ratio tend to be more efficient agents in these processes (Rose, 1977). Although magma fragmentation dictates the initial ash size distribution (Rose and Durant, 2009), in-plume and in-cloud particle aggregation can significantly alter it (Brown et al., 2012). The influences of aggregation on ash size distribution and thus, on physical chemistry of the ash–gas–aerosol interactions could be notable and is the topic of on-going investiga-

ACPD
14, 32535–32581, 2014

tions. Another important factor is the time that ash particle spend in different zones of the plume and cloud. Dynamics of the eruption as well as the ambient environmental conditions govern the spatial and temporal evolution of the eruption plume and cloud (Sparks et al., 1997). Impacts of these factors on ash chemistry could be constrained by incorporating the chemistry modules into dynamical models of volcanic eruption plumes.

Aqueous chemistry, stratospheric chemistry and all the processes involving ice could also significantly affect the fate of the dissolved iron (e.g., SO_2 oxidation catalyzed by Fe ions Harris et al., 2013). Therefore, further modeling and experimental studies are necessary to comprehend the impact of in-cloud processes on iron chemistry in volcanic ash.

Appendix A: Formulations of the processes

A1 Sulfuric acid condensation

The dew point of sulfuric acid is calculated using the following equation (Jeong and Levy, 2012):

$$\frac{1}{T_{\mathrm{dew}}} = 2.27\times10^{-5} - 2.94\times10^{-7}\cdot\ln(P_{\mathrm{H_2O}}) - 8.58\times10^{-6}\cdot\ln(P_{\mathrm{H_2SO_4}}) + 6.2\times10^{-6}\cdot\left\{\ln(P_{\mathrm{H_2O}})\cdot\ln(P_{\mathrm{H_2SO_4}})\right\} \quad \text{(A1)}$$

where, $P_{\mathrm{H_2O}}$ and $P_{\mathrm{H_2SO_4}}$ are partial pressures of the water vapor and sulfuric acid, respectively, in mmHg. When the temperature of the plume drops below T_{dew} sulfuric acid condenses onto the ash particles. In this study the Fuchs–Sutugin interpolation formula is used to describe the condensation rate of H_2SO_4 molecules to the ash particles (Fuchs and Sutugin, 1970). The single particle condensation coefficient is given

ACPD
14, 32535–32581, 2014

by:

$$K_{FS} = \alpha K_{kin}\left[1 + \frac{3\alpha}{4Kn} \times \left(1 - 0.623\frac{Kn}{1+Kn}\right)\right]^{-1} \quad \text{(A2)}$$

where

α = the accommodation coefficient of H_2SO_4 (~ 1 in this study, Clement et al., 1996),

K_{kin} = the kinetic condensation coefficient = $\pi R_p^2 c_b$,

c_b = the average thermal velocity of H_2SO_4 gas molecules = $[8kT/\pi M]^{1/2}$,

Kn = the particle Knudsen number = l/R_p,

l = the mean free path of H_2SO_4 molecules = $3D_b/c_b$,

D_b = the H_2SO_4 diffusion coefficient = $0.08\,cm^2\,s^{-1}$,

T = the absolute temperature in K,

k = the Boltzmann's constant,

M = the mass of H_2SO_4 molecule and

R_p = the particle radius.

With respect to the previous section, we calculate the condensation rate onto a polydisperse ash distribution. In that case, the condensation coefficient X_c is defined as:

$$X_c = \int_0^\infty K_{FS}(R_p)n(R_p)dR_p \quad \text{(A3)}$$

where $n(R_p)dR_p$ is the concentration of particles with radius between R_p and $R_p + dR_p$ according to Rose and Durant (2009). The condensation rate onto a polydisperse

ACPD
14, 32535–32581, 2014

distribution is finally given by:

$$CS = \int_0^\infty K_{FS}(R_p) n(R_p) \times [N_g - N_g^e(R_p)] dR_p \quad \text{(A4)}$$

where N_g is the H_2SO_4 vapor pressure in the gas phase and $N_g^e(R_p)$ is the equilibrium vapor pressure over a particle with radius R_p. In a volcanic eruption plume $N_g^e(R_p)$ is negligible in comparison to N_g. Hence Eq. (A4) simplifies to:

$$CS = X_c N_g \quad \text{(A5)}$$

A2 Water condensation

The mass-flux of water condensing onto a single, spherical particle with radius R_p is given by (Jacobson, 2005):

$$K_{FW} = \frac{4\pi D_v (p_v - p_{v,s})}{\frac{D_v L_e p_{v,s}}{k_a T}\left(\frac{L_e}{R_v T} - 1\right) + R_v T} \quad \text{(A6)}$$

where

D_v = the molecular diffusion coefficient of water vapor in air = $0.234\,cm^2\,s^{-1}$,

p_v = the vapor pressure of water vapor in plume in hPa,

$p_{v,s}$ = the saturation vapor pressure at the particle surface
$= 6.112 \exp(17.67 T_c/(T_c + 243.5))$,

T_c = the temperature in °C,

L_e = the latent heat of water evaporation = $2260\,J\,g^{-1}$,

R_v = the gas constant for water vapor = $461.40\,J\,kg^{-1}\,K^{-1}$,

ACPD
14, 32535–32581, 2014

k_a = the thermal conductivity of moist air $\approx k_d \left[1 - (1.17 - 1.02\frac{k_v}{k_d})\frac{n_v}{n_v + n_d}\right]$,

k_d, k_v = the thermal conductivities of dry air and water vapor, respectively and

n_d, n_v = the number of mol of dry air and water vapor, respectively.

Finally, the condensation rate of water onto a polydisperse aerosol distribution is calculated by:

$$CW = \int_0^\infty K_{FW}(R_p) n(R_p) dR_p \quad \text{(A7)}$$

A3 Thermodynamic equilibrium

Thermodynamic equilibrium reactions are shown in Table A2. The equilibrium coefficient (K_{eq}) for each reaction at temperature T is calculated by (Jacobson, 2005):

$$K_{eq}(T) = A \exp\left\{B\left(\frac{T_0}{T} - 1\right) + C\left(1 - \frac{T_0}{T} + \ln\frac{T_0}{T}\right)\right\} \quad \text{(A8)}$$

where $T_0 = 298.15$ K. A, B and C values are listed in Table A2.

A4 Ash dissolution

The dissolution rate of mineral species i is calculated based on a simplified formulation proposed by Palandri and Kharaka (2004):

$$\log D_i = \log k_i - n_i \cdot \text{pH} \quad \text{(A9)}$$

where D_i is the dissolution rate in mol m^{-2} s^{-1}, $\log k_i$ is the log rate constant computed at 25 °C and pH = 0, n is the reaction order with respect to H^+. Table A3 shows the

ACPD
14, 32535–32581, 2014

rate parameters used in this study for different ash constituents. These parameters are accurate to a first order approximation over the range of acidic pH (Palandri and Kharaka, 2004). We note that the dissolution rates used here (Eq. A9) are temperature independent which is a valid assumption if one considers the short residence time of particles at a certain temperature in eruption column (few seconds).

Acknowledgements. We thank P. Delmelle and P. Ayris for the discussions about volcanic processes. This work is supported through the Cluster of Excellence CliSAP (EXC177) and School of Integrated Climate System Sciences (SICSS), Universität Hamburg.

References

Achterberg, E. P., Moore, C. M., Henson, S. A., Steigenberger, S., Stohl, A., Eckhardt, S., Avendano, L. C., Cassidy, M., Hembury, D., Klar, J. K., Lucas, M. I., Macey, A. I., Marsay, C. M., and Ryan-Keogh, T. J.: Natural iron fertilization by the Eyjafjallajökull volcanic eruption, Geophys. Res. Lett., 40, 921–926, doi:10.1002/grl.50221, 2013. 32537

Atkins, P. W.: Physical Chemistry, Oxford Univ. Press, New York, 1986. 32547

Ayris, P. M. and Delmelle, P.: Volcanic and atmospheric controls on ash iron solubility: a review, Phys. Chem. Earth, 45–46, 103–112, 2012. 32538, 32539, 32543

Ayris, P. M., Lee, A. F., Wilson, K., Kueppers, U., Dingwell, D. B., and Delmelle, P.: SO_2 sequestration in large volcanic eruptions: high-temperature scavenging by tephra, Geochim. Cosmochim. Ac., 110, 58–69, 2013. 32538, 32540, 32555, 32566, 32574

Ayris, P. M., Delmelle, P., Cimarelli, C., Maters, E. C., Suzuki, Y. J., and Dingwell, D. B.: HCl uptake by volcanic ash in the high temperature eruption plume: mechanistic insights, Geochim. Cosmochim. Ac., 144, 188–201, doi:10.1016/j.gca.2014.08.028, 2014. 32538, 32540

Bagnato, E., Aiuppa, A., Bertagnini, A., Bonadonna, C., Cioni, R., Pistolesi, M., Pedone, M., and Hoskuldsson, A.: Scavenging of sulphur, halogens and trace metals by volcanic ash: the 2010 Eyjafjallajökull eruption, Geochim. Cosmochim. Ac., 103, 138–160, doi:10.1016/j.gca.2012.10.048, 2013. 32537

Bandstra, J. Z., Buss, H. L., Campen, R. K., Liermann, L. J., Moore, J., Hausrath, E. M., Navarre-Sitchler, A. K., Jang, J. H., and Brantley, S. L.: Chap. Appendix: compilation of

ACPD
14, 32535–32581, 2014

mineral dissolution rates, in: Kinetics of Water Rock Interactions, Springer, 731–733, 2007. 32573
Bayhurst, G. K., Wohletz, K. H., and Mason, A. S.: Chap. A method for characterizing volcanic ash, in: Volcanic ash and aviation safety: Proceedings of the First International Symposium on Volcanic Ash and Aviation Safety, p. 16, USGS, 1991. 32545
Blesa, M. A., Morando, P. J., and Regazzoni, A. E.: Chemical Dissolution of Metal Oxides, CRC Press, 1994. 32553
Bobrowski, N., von Glasow, R., Aiuppa, A., Inguaggiato, S., Louban, I., Ibrahim, O. W., and Platt, U.: Reactive halogen chemistry in volcanic plumes, J. Geohys. Res.-Atmos., 112, D06311, doi:10.1029/2006JD007206, 2007. 32539
Brown, R. J., Bonadonna, C., and Durant, A. J.: A review of volcanic ash aggregation, Phys. Chem. Earth, 45, 65–78, 2012. 32555
Delmelle, P., Villieras, F., and Pelletier, M.: Surface area, porosity and water adsorption properties of fine volcanic ash particles, B. Volcanol., 67, 160–169, 2005. 32544, 32545
Delmelle, P., Lambert, M., Dufrene, Y., Gerin, P., and Óskarsson, N.: Gas/aerosol/ash interaction in volcanic plumes: new insights from surface analyses of fine ash particles, Earth Planet. Sc. Lett., 259, 159–170, 2007. 32537, 32539, 32548, 32551
Dingwell, D. B., Lavallee, Y., and Kueppers, U.: Volcanic ash: a primary agent in the Earth system, Phys. Chem. Earth, 45–46, 2–4, doi:10.1016/j.pce.2011.07.007, 2012. 32537
Duggen, S., Olgun, N., Croot, P., Hoffmann, L., Dietze, H., Delmelle, P., and Teschner, C.: The role of airborne volcanic ash for the surface ocean biogeochemical iron-cycle: a review, Biogeosciences, 7, 827–844, doi:10.5194/bg-7-827-2010, 2010. 32539, 32545, 32553
Fuchs, N. A. and Sutugin, A. G.: Highly Dispersed Aerosols, Ann Arbor Science Publ., Ann Arbor, Michigan, 1970. 32556
Hamme, R. C., Webley, P. W., Crawford, W. R., Whitney, F. A., DeGrandpre, M. D., Emerson, S. R., Eriksen, C. C., Giesbrecht, K. E., Gower, J. F. R., Kavanaugh, M. T., Panea, M. A., Sabine, C. L., Batten, S. D., Coogan, L. A., Grundle, D. S., and Lockwood, D.: Volcanic ash fuels anomalous plankton bloom in subarctic northeast Pacific, Geophys. Res. Lett., 37, L19604, doi:10.1029/2010GL044629, 2010. 32537
Harris, E., Sinha, B., van Pinxteren, D., Tilgner, A., Fomba, K. W., Schneider, J., Roth, A., Gnauk, T., Fahlbusch, B., Mertes, S., Lee, T., Collett, J., Foley, S., Borrmann, S., Hoppe, P., and Herrmann, H.: Enhanced role of transition metal ion catalysis during in-cloud oxidation of SO_2, Science, 340, 727–730, 2013. 32556

ACPD
14, 32535–32581, 2014

Heiken, G. and Wohletz, K.: Volcanic Ash, University of California Press, London, 1992. 32537
Hort, M. and Gardner, J.: Constraints on cooling and degassing of pumice during Plinian volcanic eruptions based on model calculations, J. Geophys. Res.-Sol. Ea., 115, 25981–26001, 2000. 32541, 32566
Horwell, C. J., Fenoglio, I., Ragnarsdottir, K. V., Sparks, R. S. J., and Fubini, B.: Surface reactivity of volcanic ash from the eruption of Soufrire Hills volcano, Montserrat, West Indies with implications for health hazards, Environ. Res., 93, 202–215, doi:10.1016/S0013-9351(03)00044-6, 2003. 32537
Hoshyaripour, G., Hort, M., and Langmann, B.: How does the hot core of a volcanic plume control the sulfur speciation in volcanic emission?, Geochem. Geophy. Geosy., 13, 100–115, 2012. 32543
Hoshyaripour, G., Hort, M., Langmann, B., and Delmelle, P.: High temperature volcanic controls on ash iron solubility: new insights from high-temperature gas–ash interaction modeling, J. Volcanol. Geoth. Res., 286, 67–77, 2014. 32538, 32540, 32550, 32555, 32574
Höskuldsson, A., Óskarsson, N., Pedersen, R., Grönvold, K., Vogfjörò, K., and Ólafsdóttir, R.: The millennium eruption of Hekla in February 2000, B. Volcanol., 70, 169–182, 2007. 32552
Jacobson, M. Z.: Fundamentals of Atmospheric Modeling, Cambridge University Press, 2005. 32543, 32558, 32559, 32571, 32572
Jeong, K. and Levy, E. K.: Theoretical prediction of sulfuric acid condensation rates in boiler flue gas, Int. J. Heat Mass Tran., 55, 8010–8019, doi:10.1016/j.ijheatmasstransfer.2012.08.037, 2012. 32556
Jeong, D., Kim, K., and Choi, W.: Accelerated dissolution of iron oxides in ice, Atmos. Chem. Phys., 12, 11125–11133, doi:10.5194/acp-12-11125-2012, 2012. 32555
Jones, M. T. and Gislason, S. R.: Rapid releases of metal salts and nutrients following the deposition of volcanic ash into aqueous environments, Geochim. Cosmochim. Ac., 72, 3661–3680, 2008. 32551, 32552, 32570, 32581
Langmann, B., Zakšek, K., Hort, M., and Duggen, S.: Volcanic ash as fertiliser for the surface ocean, Atmos. Chem. Phys., 10, 3891–3899, doi:10.5194/acp-10-3891-2010, 2010. 32537, 32538, 32553
Larkin, K.: Canada sees shock salmon glut, Nature News, September 2010, doi:10.1038/news.2010.449, 2010. 32536
Lindsley, D. H.: Oxide Minerals: Petrologic and Magnetic Significance, vol. 25, Mineralogical Society of America Reviews in Mineralogy, 1991. 32554

ACPD
14, 32535–32581, 2014

Mastin, L. G.: A user-friendly one-dimensional model for wet volcanic plumes, Geochem. Geophy. Geosy., 8, Q03014, doi:10.1029/2006GC001455, 2007. 32541
Meskhidze, N., Chameides, W. L., and Nenes, A.: Dust and pollution: a recipe for enhanced ocean fertilization?, J. Geohys. Res.-Atmos., 110, D03301, doi:10.1029/2004JD005082, 2005. 32542
Mills, O. P. and Rose, W. I.: Shape and surface area measurements using scanning electron microscope stereo-pair images of volcanic ash particles, Geosphere, 6, 805–811, 2010. 32545
Moune, S., Gauthier, P. J., Gislason, S. R., and Sigmarsson, O.: Trace element degassing and enrichment in the eruptive plume of the 2000 eruption of Hekla volcano, Iceland, Geochim. Cosmochim. Ac., 70, 461–479, 2006. 32551, 32552
Moune, S., Sigmarsson, O., Thordarson, T., and Gauthier, P. J.: Recent volatile evolution in the magmatic system of Hekla volcano, Iceland, Earth Planet. Sc. Lett., 255, 373–389, 2007. 32551, 32552
Moune, S., Holtz, F., and Botcharnikov, R. B.: Sulphur solubility in andesitic to basaltic melts: implications for Hekla volcano, Contrib. Mineral. Petr., 157, 691–707, 2009. 32554
Nakagawa, M. and Ohba, T.: Minerals in volcanic ash 1: Primary minerals and volcanic glass, Global Environ. Res., 6, 41–50, 2003. 32545, 32546, 32549
Naughton, J. J., Lewis, V. A., Hammond, D., and Nishimoto, D.: The chemistry of sublimates collected directly from lava fountains at Kilauea volcano, Hawaii, Geochim. Cosmochim. Ac., 38, 1670–1690, 1974. 32548
Oelkers, E. H. and Gislason, S. R.: The mechanism, rates and consequences of basaltic glass dissolution: I. An experimental study of the dissolution rates of basaltic glass as a function of aqueous Al, Si, and oxalic acid concentration at 25 °C and pH = 3 and 11, Geochim. Cosmochim. Ac., 65, 3671–3681, 2001. 32573
Olgun, N., Duggen, S., Croot, P. L., Delmelle, P., Dietze, H., Schacht, U., Oskarsson, N., Siebe, C., Auer, A., and Garbe-Schonberg, D.: Surface ocean iron fertilization: the role of airborne volcanic ash from subduction zone and hot spot volcanoes and related iron fluxes into the Pacific Ocean, Global. Biogeochem. Cy., 25, GB4001, doi:10.1029/2009GB003761, 2011. 32548, 32553
Olgun, N., Duggen, S., Langmann, B., Hort, M., Waythomas, C. F., Hoffmann, L. J., and Croot, P.: Geochemical evidence of oceanic iron fertilization by the Kasatochi volcanic eruption in 2008 and the potential impacts on Pacific sockeye salmon, Mar. Ecol.-Prog. Ser., 488, 81–88, 2013a. 32537

ACPD
14, 32535–32581, 2014

Olgun, N., Duggen, S., Andronico, D., Kutterolf, S., Croot, P. L., Giammanco, S., Censi, P., and Randazzo, L.: Possible impacts of volcanic ash emissions of Mount Etna on the primary productivity in the oligotrophic Mediterranean Sea: results from nutrient-release experiments in seawater, Mar. Chem., 152, 32–42, 2013b. 32537, 32553

Óskarsson, N.: The interaction between volcanic gases and tephra: fluorine adhering to tephra of the 1970 Hekla eruption, J. Volcanol. Geoth. Res., 8, 251–266, 1980. 32539, 32546, 32547, 32552

Palandri, J. L. and Kharaka, Y. K.: A Compilation of Rate Parameters of Water–Mineral Interaction Kinetics for Application to Geochemical Modeling, USGS, 2004. 32554, 32559, 32560, 32573

Parsons, T. R. and Whitney, F. A.: Did volcanic ash from Mt. Kasatoshi in 2008 contribute to a phenomenal increase in Fraser River sockeye salmon (*Oncorhynchus nerka*) in 2010?, Fish. Oceanogr., 21, 374–377, doi:10.1111/j.1365-2419.2012.00630.x, 2012. 32536

Pirjola, L., Kulmala, M., Wilck, M., Bischoff, A., Stratmann, F., and Otto, E.: Formation of sulphuric acid aerosols and cloud condensation nuclei: an expression for significant nucleation and model comparison, J. Aerosol. Sci., 30, 1079 –1094, doi:10.1016/S0021-8502(98)00776-9, 1999. 32544

Rose, W. I.: Scavenging of volcanic aerosol by ash: atmospheric and volcanologic implications, Geology, 5, 621–624, 1977. 32547, 32555

Rose, W. I. and Durant, A. J.: Total grain size distribution of explosive volcanic eruptions., J. Volcanol. Geoth. Res., 186, 32–39, 2009. 32537, 32544, 32545, 32555, 32557, 32566, 32575

Sander, S. P., Abbatt, J., Barker, J. R., Burkholder, J. B., Friedl, R. R., Huie, D. M. G. R. E., Kolb, C. E., Kurylo, M. J., Moortgat, G., Orkin, V. L., and Wine, P. H.: Chemical kinetics and photochemical data for use in atmospheric studies, Evaluation No. 17, Jet Propulsion Laboratory, Pasadena, 2011. 32571

Schmincke, H. U.: Volcanism, Springer-Verlag, Berlin, Heidelberg, 2004. 32545

Seinfeld, J. H. and Pandis, S. N.: Atmospheric Chemistry and Physics: From Air Pollution to Climate Change, John Wiley and Sons, New York, 2006. 32540, 32571

Shampine, L. F. and Reichelt, M. W.: The MATLAB ODE Suite, SIAM J. Sci. Comput., 18, 1–22, 1997. 32542

ACPD
14, 32535–32581, 2014

Sparks, R. S. J., Bursik, M. I., Carey, S. N., Gilbert, J. S., Glaze, L. S., Siggurdsson, H., and Woods, A. W.: Volcanic Plumes, John Wiley and Sons, New York, 1997. 32544, 32545, 32556

Symonds, R. B., Rose, W. I., Bluth, G. J. S., and Gerlach, T. M.: Chap. Volcanic gas studies: methods, results and applications, in: Volatiles in Magma, , Reviews in Mineralogy, vol. 30. American Mineralogical Society, 1–66, 1994. 32543, 32549, 32553

Tabazadeh, A. and Turco, R. P.: Stratospheric chlorine injection by volcanic eruptions: HCl scavenging and implications for ozone, Science, 260, 1082–1086, 1993. 32539, 32541, 32547

Textor, C., Graf, H. F., Herzog, M., and Oberhuber, J. M.: Injection of gases into the stratosphere by explosive volcanic eruptions, J. Geophys. Res.-Atmos., 108, 4606, doi:10.1029/2002JD002987, 2003. 32539, 32540, 32547, 32554, 32555

Textor, C., Graf, H., Longo, A., Neri, A., Ongaro, T. E., Papale, P., Timmreck, C., and Ernst, G. G. J.: Numerical simulation of explosive volcanic eruptions from the conduit flow to global atmospheric scales, Ann. Geophys.-Italy, 48, 817–842, 2005. 32537

Textor, C., Graf, H. F., Herzog, M., Oberhuber, J., Rose, W. I., and Ernst, G. G. J.: Volcanic particle aggregation in explosive eruption columns. Part II: Numerical experiments, J. Volcanol. Geoth. Res., 150, 378–394, doi:10.1016/j.jvolgeores.2005.09.008, 2006a. 32539

Textor, C., Graf, H. F., Herzog, M., Oberhuber, J. M., Rose, W. I., and Ernst, G. G. J.: Volcanic particle aggregation in explosive eruption columns. Part I: Parameterization of the microphysics of hydrometeors and ash, J. Volcanol. Geoth. Res., 150, 359–377, doi:10.1016/j.jvolgeores.2005.09.007, 2006b. 32539, 32540

US Committee on Extension to the Standard Atmosphere: U.S. Standard Atmosphere, Natl. Oceanic and Atmos. Admin., Washington, D. C., 1976. 32541

Verhoff, F. H. and Banchero, J. T.: Predicting dew points of gases, Chem. Eng. Prog., 78, 71–72, 1974. 32543, 32546

Wang, B., Michaelson, G., Ping, C., Plumlee, G., and Hageman, P.: Characterization of pyroclastic deposits and pre-eruptive soils following the 2008 eruption of Kasatochi Island Volcano, Alaska, Arct. Antarct. Alp. Res., 42, 276–284, 2010. 32553

Wolff-Boenisch, D., Gislason, S. R., and Oelkers, E. H.: The effect of fluoride on the dissolution rates of natural glasses at pH 4 and 25 °C, Geochim. Cosmochim. Ac., 68, 4571–4582, 2004. 32551

ACPD
14, 32535–32581, 2014

Table 1. Different zones of the plume that affect the fine ash during a plinian and sub-plinian volcanic eruptions.

Zone	Location	Subzones	Time scale [a]	Length scale	Temperature
Conduit	fragmentation level to vent	–	6–275 s	few meters to few km	$T > 600\,^{\circ}C$
Plume	vent to NBL	high-T[b] mid-T low-T	150–250 s	few km to tens of km	> ambient
Cloud	after NBL	warm[c] cold	hours to days	> hundreds of km	~ ambient

[a] From Ayris et al. (2013); Hort and Gardner (2000) and Rose and Durant (2009) for conduit, plume and cloud zones, respectively;
[b] high-T: $T > 600\,^{\circ}C$, mid-T: $150\,^{\circ}C < T < 600\,^{\circ}C$ and low-T: $50\,^{\circ}C < T < 150\,^{\circ}C$;
[c] warm zone: $T >$ freezing point (~ $0\,^{\circ}C$), cold zone: $T <$ freezing point.

ACPD
14, 32535–32581, 2014

Table 2. The major species considered in this study.

Phase	Species
Gas	H_2, H_2O, H_2O_2, SO_2, H_2S, SO_3, H_2SO_4, CO, CO_2, O_3, HF, HCl, HClO, OH, O, H, Cl, ClO, SO, HS, HSO_3, NO, NO_2, NO_3, HNO_3, NH_3, N_2, O_2
Liquid	H_2O, H_2O_2, OH, H_2SO_4, SO_2, NO_2, NO_3, HNO_3, NH_3, H^+, OH^-, SO_4^{2-}, SO_3^{2-}, HSO_4^-, HSO_3^-, Cl^-, F^-, NH_4^+, Fe^{2+}, Fe^{3+}, Al^{3+}
Solid	glass: $SiAl_{0.36}O_2$ $(OH)_{1.08}$, fayalite: Fe_2SiO_4, magnetite: Fe_3O_4, hematite: Fe_2O_3

ACPD
14, 32535–32581, 2014

Table 3. Average volcanic gas composition entering the mid-T zone (T = 600 °C after mixing of 1000 °C magmatic gas with ambient air) for convergent plate (CP) or HCl-rich, divergent plate (DP) or CO_2-rich and hot spots (HS) or SO_2-rich eruptions (concentrations are in mole%). CP composition is used in the reference scenario. DP and HS compositions are used in the sensitivity study.

Species	CP	DP	HS
H_2O	57.70	50.00	53.50
CO_2	2.80	8.50	2.20
H_2	0.01	0.01	0.01
H_2S	0.01	0.01	0.01
SO_2	0.40	1.90	3.96
SO_3	0.87	3.00	2.85
H_2SO_4	0.01	0.03	0.03
HCl	0.45	0.26	0.11
HF	0.04	0.26	0.12
CO	0.11	0.20	0.22
O_2	5.10	2.40	4.10
N_2	32.10	33.40	33.70

ACPD
14, 32535–32581, 2014

Table 4. Sensitivity of the key iron mobilization parameters to the gas and ash composition.

Sensitivity study	Gas composition (tectonics)			Ash composition			
Parameter	CP	DP	HS	A	B	C	D
Final pH	0.32	0.38	0.51	0.31	0.32	1.35	1.36
Scavenged SO_2 %	2.86	2.59	3.60	2.81	2.81	19.30	19.60
Scavenged HCl%	98.51	98.58	98.41	98.49	98.55	98.48	98.52
Scavenged HF%	12.78	12.0	16.78	12.54	12.56	61.31	61.55
Dissolved Fe^{2+}%	0.11	0.08	0.07	–	0	33	13.85
Total dissolved Fe %	0.15	0.11	0.10	–	0.03	33	13.86
Dissolution rate*	6.44	5.98	5.55	0.0002	0.6	220	210

* Dissolution rates are reported in $\mathrm{mol\,cm^{-2}\,s^{-1}} \times 10^{-12}$.

ACPD
14, 32535–32581, 2014

Table 5. Calculated and measured iron release from the volcanic ash surface.

Volcano	Eruption year	C_{Fe} [a] wt%	D_i range [b] wt%	Measures R_{Fe} [a] µmol g^{-1} ash	Calculated R_{Fe} [b] µmol g^{-1} ash
Galeras, Colombia	2005	7.47	0.03–0.15	0.12	0.004–0.1
Montserrat, Caribbean	2003	6.57	0.03–0.15	0.04	0.003–0.08
Hekla, Iceland	2000	11.86	13.85–33.0	10.85	2.93–34.94
Sakurajima, Japan	1994	7.96	0.03–0.15	0.03	0.004–0.10
Lascar, Chile	1993	6.0	0.03–0.15	0.01	0.003–0.08

[a] Extracted from Table 2 of Jones and Gislason (2008); [b] Based on values reported in Table 4.

ACPD
14, 32535–32581, 2014

Table A1. Gas-phase reactions and rate coefficients.

No.	Reaction	Rate coefficient	Reference*
R1	$SO_2 + 0.5O_2 \rightarrow SO_3$	$1.3 \times 10^{-33}(600/T)^{3.6}$	1, 2
R2	$SO_3 + O_3 \rightarrow SO_3 + O_2$	$3.0 \times 10^{-12}e^{-7100/T}$	1
R3	$SO_2 + OH \rightarrow HSO_3$	$4.0 \times 10^{-31}(300/T)^{3.3}$	1, 2
R4	$HSO_3 + O_2 \rightarrow SO_3 + HO_2$	$1.3 \times 10^{-12}e^{-330/T}$	1, 2
R5	$SO_3 + H_2O \rightarrow H_2SO_4$	6.0×10^{-15}	3, 2
R6	$H_2S + OH \rightarrow HS + H_2O$	$6.3 \times 10^{-12}e^{-80/T}$	1, 2
R7	$HS + O_2 \rightarrow SO + OH$	4.0×10^{-19}	3
R8	$SO + O_2 \rightarrow SO_2 + O$	$2.1 \times 10^{-13}e^{-2280/T}$	1, 2
R9	$HCl + OH \rightarrow Cl + H_2O$	$2.4 \times 10^{-12}e^{-330/T}$	1, 2
R10	$HClO + O \rightarrow ClO + OH$	$1.0 \times 10^{-11}e^{-1300/T}$	1, 2
R11	$NO + O_3 \rightarrow NO_2 + O_2$	$1.8 \times 10^{-12}e^{-1370/T}$	1, 3
R12	$OH + O \rightarrow H + O_2$	$2.3 \times 10^{-11}e^{110/T}$	1, 2
R13	$OH + O_3 \rightarrow HO_2 + O_2$	$1.9 \times 10^{-12}e^{-1000/T}$	2, 3
R14	$OH + H_2 \rightarrow H_2O + H$	$7.7 \times 10^{-12}e^{-2100/T}$	1, 2
R15	$OH + OH \rightarrow H_2O + O$	$4.2 \times 10^{-12}e^{-240/T}$	1, 3

* 1: (Sander et al., 2011), 2: (Jacobson, 2005), 3: (Seinfeld and Pandis, 2006).

ACPD
14, 32535–32581, 2014

Table A2. Equilibrium reactions and rate coefficients (Jacobson, 2005).

No.	Reaction	A	B	C
E1	$SO_2(g) \rightleftharpoons SO_2(aq)$	1.22	10.55	0
E2	$H_2O_2(g) \rightleftharpoons H_2O_2(aq)$	7.45×10^4	22.21	0
E3	$NO_2(g) \rightleftharpoons NO_2(aq)$	1.00×10^{-2}	8.38	0
E4	$NO_3(g) \rightleftharpoons NO_3(aq)$	2.10×10^5	29.19	0
E5	$OH(g) \rightleftharpoons OH(aq)$	2.50×10^1	17.12	0
E6	$HNO_3(g) \rightleftharpoons HNO_3(aq)$	2.10×10^5	0	0
E7	$NH_3(g) \rightleftharpoons NH_3(aq)$	5.76×10^1	13.79	−5.39
E8	$SO_2(aq) + H_2O \rightleftharpoons H^+ + HSO_3^-$	1.71×10^{-2}	7.04	0
E9	$HSO_3^- \rightleftharpoons H^+ + SO_3^{2-}$	5.99×10^{-8}	3.74	0
E10	$HCl(g) \rightleftharpoons H^+ + Cl^-$	$1.97 \times 10^{+6}$	30.19	19.91
E11	$HF(g) \rightleftharpoons H^+ + F^-$	3.94	25.04	16.34
E12	$NH_3(aq) + H_2O \rightleftharpoons NH_4^+ + OH^-$	1.85×10^{-5}	−1.5	0
E13	$H_2SO_4 \rightleftharpoons H^+ + HSO_4^-$	$1.00 \times 10^{+3}$	0	0
E14	$HSO_4^- \rightleftharpoons H^+ + SO_4^{2-}$	1.02×10^{-2}	8.85	25.14

ACPD
14, 32535–32581, 2014

Table A3. Ash dissolution reactions and rate parameters.

Species	Reaction	log k	n	Reference*
Fayalite	$Fe_2SiO_4 + 4H^+ \rightarrow 2Fe^{2+} + 2H_2O + SiO_2$	−5.80	1.0	1,2
Magnetite	$Fe_3O_4 + 8H^+ \rightarrow 2Fe^{2+} + Fe^{3+} + 4H_2O$	−8.59	0.279	1,2
Hematite	$Fe_2O_3 + 6H^+ \rightarrow 2Fe^{3+} + 3H_2O$	−9.39	0.421	1,2
Glass	$SiAl_{0.36}O_2(OH)_{1.08} + 1.08H^+ \rightarrow SiO_2 + 0.36Al^{3+} + 1.08H_2O$	−12.30	–	3

* 1: (Palandri and Kharaka, 2004), 2: (Bandstra et al., 2007), 3: (Oelkers and Gislason, 2001).

ACPD
14, 32535–32581, 2014

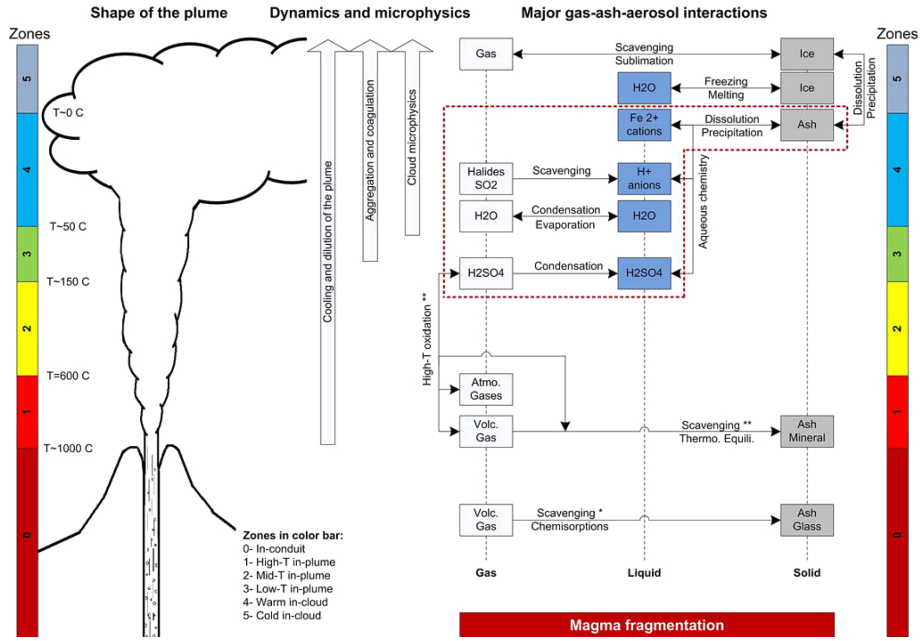

Figure 1. The interaction between ash surface, liquid coating and the surrounding gases. During high-T zones (zones 0 and 1 in the color bar) direct gas–ash interaction significantly controls the iron speciation at the ash surface. At lower temperatures, however (zones 2, 3, 4 and 5), such interactions are negligible. The formation of liquid coating at the ash surface and its interactions with the surrounding gases (scavenging) and with the ash constituents (dissolution) mainly control the ash iron mobilization. Only the processes within the red dotted-line are considered in this study (* Ayris et al., 2013; ** Hoshyaripour et al., 2014)

ACPD
14, 32535–32581, 2014

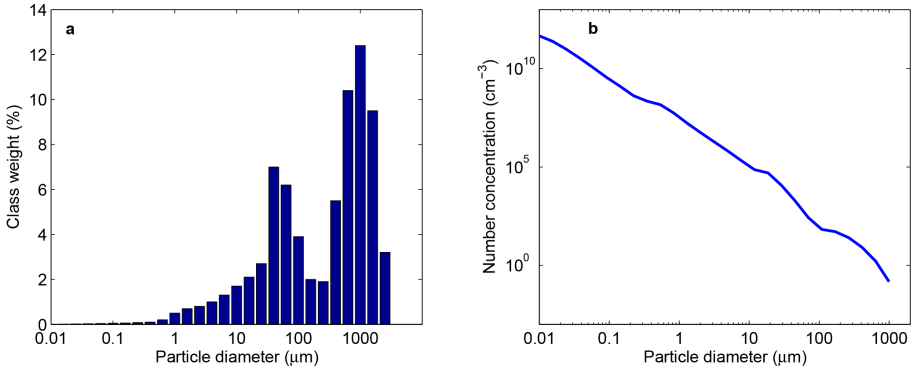

Figure 2. (a) Typical distal ash-fall particle size analysis from Rose and Durant (2009), **(b)** particle number concentration calculated based on the same data.

ACPD
14, 32535–32581, 2014

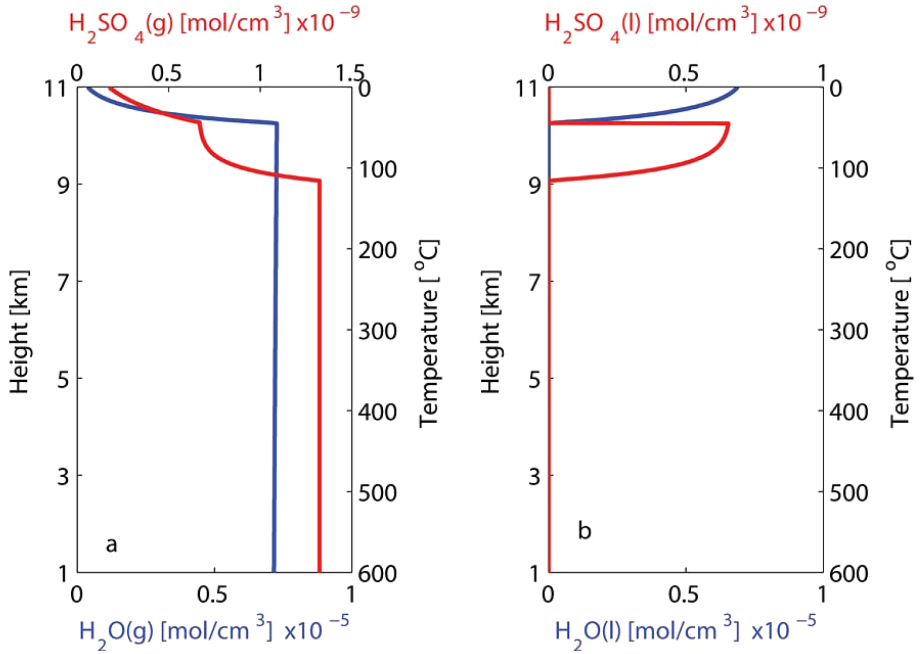

Figure 3. Vertical profile of the water (blue line) and sulfuric acid (red line) concentrations in the **(a)** gas and **(b)** aqueous phases in the eruption plume. Please note the significant differences between H_2O and H_2SO_4 concentration. Vertical axis on left and right show the elevation and the plume temperature, respectively.

ACPD
14, 32535–32581, 2014

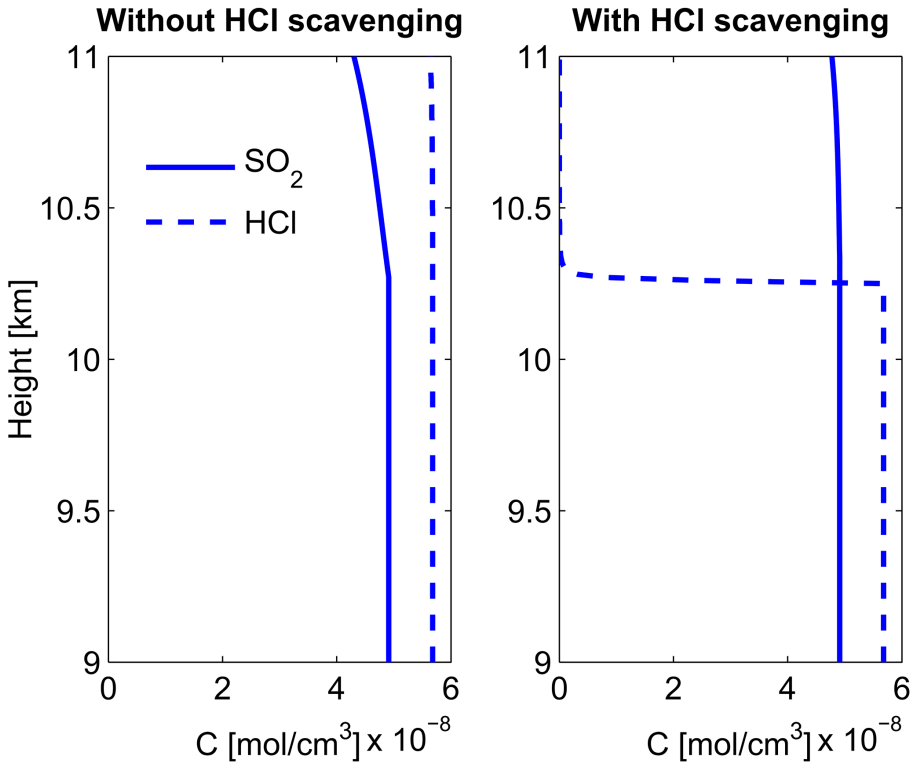

Figure 4. SO_2 and HCl vertical profile. Left panel: without HCl scavenging (e.g., very low halide concentration in sulfur rich plumes); right panel: with HCl scavenging (e.g., HCl-rich plumes). Note that only the height > 9 km is plotted here.

ACPD
14, 32535–32581, 2014

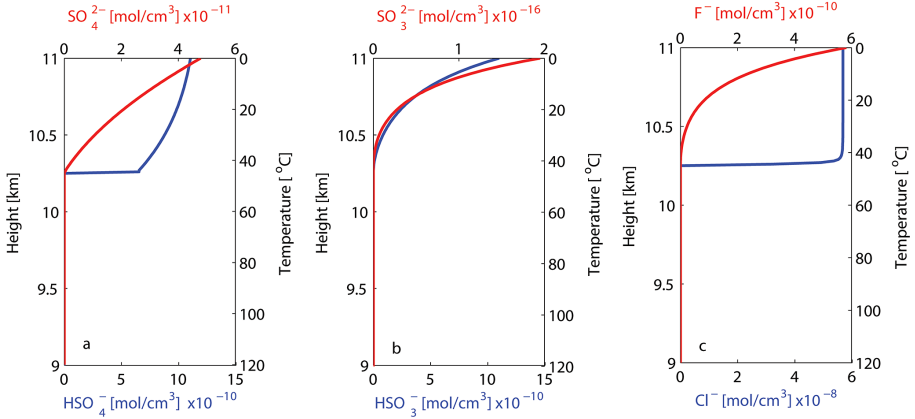

Figure 5. Vertical profile of the concentrations of major anions formed in the aqueous phase: **(a)** HSO_4^- and SO_2^{2-} that form due to sulfuric acid dissociation. **(b)** HSO_3^- and SO_3^{2-} are the products of SO_2 scavenging and dissociation. **c)** Cl^- and F^- that are produced due to HCl and HF dissociation, respectively. Please note the different concentration scales. Vertical axis on left and right show the elevation and the plume temperature, respectively. Note that only the height > 9 km is plotted here.

ACPD
14, 32535–32581, 2014

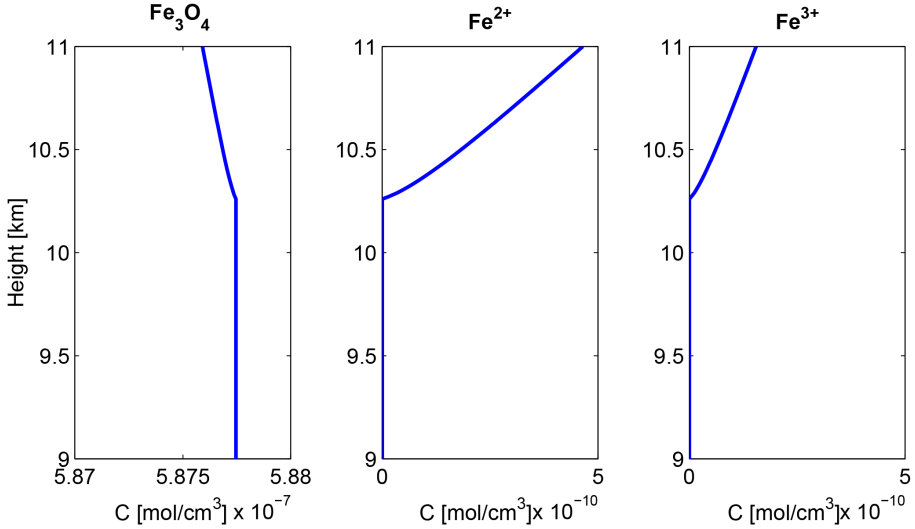

Figure 6. Vertical profile of magnetite (Fe_3O_4), iron II and iron III concentrations. Because of relatively slow dissolution rate in the reference scenario, changes in magnetite concentration are small. Note that only the height > 9 km is plotted here.

ACPD
14, 32535–32581, 2014

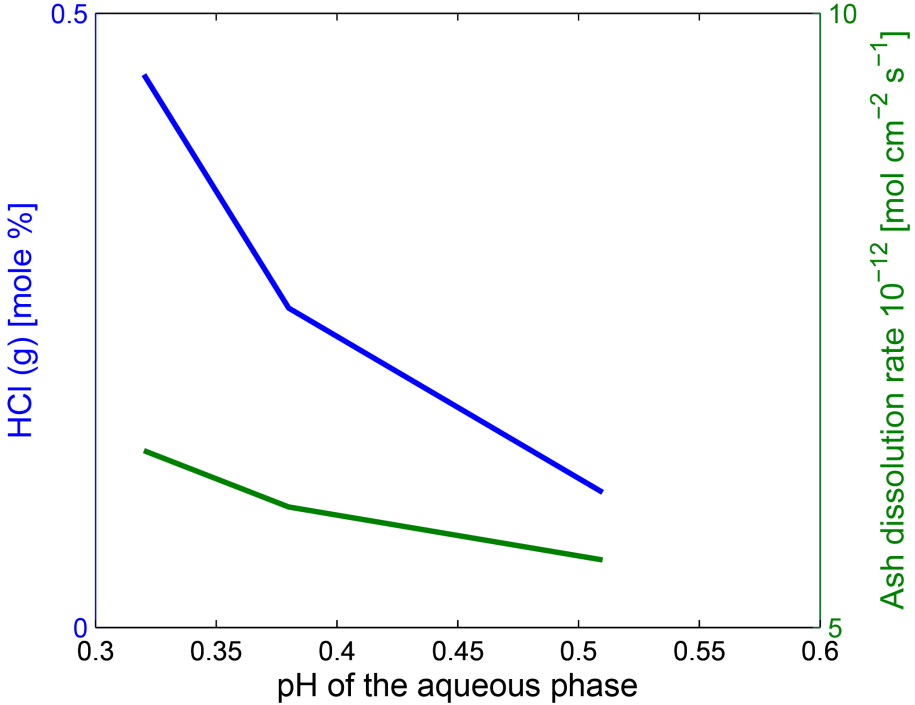

Figure 7. Correlation between pH, HCl content of the magmatic gas and the ash dissolution rate.

ACPD
14, 32535–32581, 2014

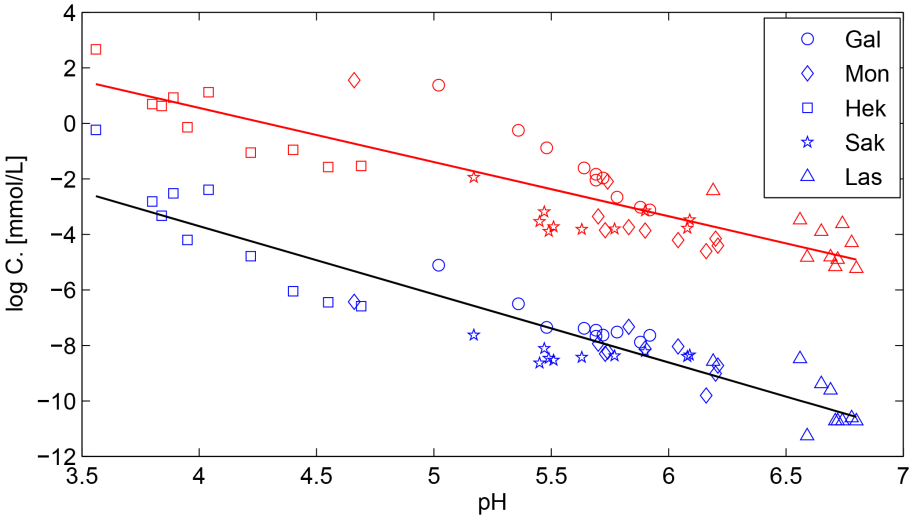

Figure 8. Concentration of iron (blue) and halogens (Cl + F in red) released form ash samples during leaching experiment of Jones and Gislason (2008) as function of pH. Solid lines only show the trends.

ACPD
14, 32535–32581, 2014